Calcination under low CO_2 pressure enhances the Calcium Looping performance of limestone for thermochemical energy storage

Beatriz Sarrión[a], Antonio Perejón[a,b,*], Pedro E. Sánchez-Jiménez[a], Nabil Mohamed Amghar[a], Ricardo Chacartegui[c], José Manuel Valverde[d], Luis A. Pérez-Maqueda[a]

[a]Instituto de Ciencia de Materiales de Sevilla (C.S.I.C.-Universidad de Sevilla). C. Américo Vespucio 49, Sevilla 41092. Spain.

[b]Departamento de Química Inorgánica, Facultad de Química, Universidad de Sevilla, Sevilla 41071, Spain.

[c]Departamento de Ingeniería Energética, Escuela Técnica Superior de Ingeniería, Universidad de Sevilla, 41092 Sevilla, Spain

[d]Faculty of Physics, University of Seville, Avenida Reina Mercedes s/n, 41012 Sevilla, Spain.

Abstract

The Calcium Looping performance of limestone for thermochemical energy storage has been investigated under novel favorable conditions, which involve calcination at moderate temperature under CO_2 at low pressure (0.01 and 0.1 bar) and carbonation at high temperature under CO_2 at atmospheric pressure. Calcining at low CO_2 pressures allows to substantially reducing the temperature to achieve full calcination in short residence times. Moreover, it notably enhances CaO multicycle conversion. The highest values of conversion are obtained for limestone samples calcined under 0.01 bar CO_2 at 765ºC. Under these conditions, residual conversion is increased by a factor of 10 as compared to conditions involving calcination under CO_2 at atmospheric pressure. The enhancement of CaO conversion is correlated to the microstructure of the CaO samples

obtained after calcination. As seen from SEM, BET surface and XRD analysis calcination under low CO_2 pressure leads to a remarkably decrease of pore volume and CaO crystallite size. Consequently, CaO surface area available for carbonation in the fast reaction-controlled regime and therefore reactivity in short residence times is promoted.

Keywords: Concentrated Solar Power; limestone; thermochemical energy storage; Calcium-Looping; low CO_2 pressure

Corresponding author:

antonio.perejon@icmse.csic.es

1. Introduction

Thermochemical energy storage (TCES) systems, based upon the heat absorbed and released in reversible chemical reactions with high turning temperature, have a great potential in concentrated solar power (CSP) plants [1-3]. One of the main advantages of TCES is that it allows decoupling the generation of power from demand. In general terms, heat generated in the CSP plant is used to carry out a reversible endothermic chemical reaction whose byproducts are stored separately. On demand, the exothermic reverse reaction is triggered, which releases the chemically stored heat to be used for generating electrical power [4-6].

The Calcium-Looping (CaL) process, based on the decarbonation and carbonation reactions of calcium carbonate ($CaCO_3$/CaO) is being currently the subject of several lab-scale and process engineering studies for thermochemical energy storage in CSP plants with tower technology (CaL-TCES), with small pilot scale plants under construction [7-

18]. Large pilot-scale demonstrations (1-2 MWth) have already shown that the CaL process can be an efficient low cost technology to capture CO_2 from fossil fuel thermoelectric plants [19-21]. The CaL process for CO_2 capture and storage (CaL-CCS) is based on the carbonation reaction of CaO to capture CO_2 from flue gases at temperatures around 650ºC and the subsequent regeneration of the carbonated solids by calcination at temperatures above 900ºC in a high CO_2 concentration environment [22, 23]. In the CaO capture process carried out in the carbonator, the post-combustion gas (with a CO_2 concentration of ~15%vol. at atmospheric pressure) is used to fluidize a bed of CaO particles. The now partially carbonated particles are then transported to a second fluidized bed reactor (calciner) where calcination proceeds in short residence times. In this way, the CO_2 resulting from the combustion of fossil fuels is recovered in the calciner at high concentration to be subsequently compressed and stored or transported for other uses. After calcination, the regenerated CaO is circulated back to the carbonator for its use in a new cycle [24, 25]. The efficiency of the CaL technology for CO_2 capture is limited though by process conditions, such as the low CO_2 concentration in the post-combustion gases and the necessarily short residence times in the reactor due to the high mass flow rates involved [26]. Moreover, the high temperatures and high CO_2 concentration in the calciner, added to inactivation by irreversible sulphation and ashes, greatly reduce the reactivity of the regenerated CaO in each cycle [27]. These adverse conditions lead to an irreversible rapid loss of CaO reactivity with the number of cycles [28-30].

The proposed integration of the CaL technology in CSP plants as a TCES system is based also on the reversibility and endothermic nature of the $CaCO_3$ decarbonation reaction [7, 8]. $CaCO_3$ has a significantly higher energy density than that of molten salts, currently used as the state-of-the-art thermal energy storage system in CPS commercial plants [8,

31-33]. Moreover, molten salts have serious limitations, such as a limited maximum operation temperature (550ºC to avoid degradation), their high cost, the need of storage temperature above a certain minimum (150-200ºC) to avoid solidification and the corrosion caused in the materials used to transport and storage these fluids [34-36]. On the other hand, natural $CaCO_3$ rich minerals such as limestone and dolomite are non-toxic, very abundant and inexpensive. In addition, both calcium carbonate and the calcium oxide obtained after calcination can be stored indefinitely without thermal losses [8, 37, 38].

It must be remarked that the most adequate calcination/carbonation conditions in the CaL-CSP integration are not necessarily the same as in the CaL-CCS process since the reversibility of the process permits to adjust the working temperatures depending on the CO_2 partial pressure, and according to the thermodynamic equilibrium of the reaction [7, 39]. Thus, it has been proposed to carry out carbonation at a high temperature (> 800ºC) in an environment of high CO_2 concentration, while the calcination temperature could be lowered using inert gases, atmospheres with a low concentration of CO_2 or low CO_2 pressures to avoid CaO deactivation [8].

In the CaL-TCES process, concentrated solar energy is used to decompose $CaCO_3$ at high temperatures on a bed or stream of particles in a solar reactor. The products of the reaction, CaO and CO_2, are then transported and stored separately. When energy production is demanded, these products are circulated to a fluidized bed reactor to carry out the exothermic carbonation reaction. The CO_2 in excess over the stoichiometric need is released as a high pressure and high temperature stream from the carbonator to a gas turbine for power production using a CO_2 closed cycle. Thus, carbonation should be ideally carried out at high temperature and high CO_2 pressure to enhance the thermoelectric efficiency of the cycle [10, 40-42]. On the other hand, a variety of

calcination conditions and types of reactors have been proposed in the literature [8, 16, 43-45]. One possibility is using helium in the calciner atmosphere, which greatly reduces the calcination temperature in short residence times below ~725ºC and could be separated from the CO_2 released during calcination using state of the art membrane technologies [37, 46]. Calcination at this low temperature would reduce the loss of multicycle CaO activity caused by sintering. However, the need of adding a CO_2-He separation step increases the technical complexity, energy penalty and cost of the technology [15, 16]. A further option is to calcine under pure CO_2, which would simplify the process, as it would allow carrying out the whole cycle through a closed CO_2 circuit. In this case, the greatest inconvenient would be the rapid decay of CaO activity with the number of cycles [10, 15]. In order to achieve complete calcination of $CaCO_3$ under pure CO_2 at atmospheric pressure the temperatures required are around 950ºC which promotes sintering-induced deactivation of the CaO particles. Consequently, CaO reactivity is considerably decreased in each cycle as seen in the CaL-CCS process [15, 22].

As demonstrated in recent works having data on the multicycle CaL activity of the CaO precursor at realistic process conditions is of paramount relevance for plant modelling analysis to yield reliable results. Thus, lab-scale experimental measurements should be performed at practical conditions imposed by the process. Regarding calcination in the CaL-TCES system a further possibility suggested in the engineering literature is using a pure CO_2 environment at reduced absolute pressure, which is technically feasible still allowing to carry out the whole process in a closed CO_2 circuit [16, 47]. Expectedly, the calcination temperature could be decreased at reduced absolute CO_2 pressure thus mitigating the decay of CaO activity with the number of cycles [48]. Up to our knowledge there are no studies reporting the multicyclic behavior of CaO precursors involving calcination at reduced CO_2 absolute pressure. This is the main goal of the present study.

2. Materials and methods

2.1. Materials

Natural limestone of high purity (99.3 wt% $CaCO_3$) received from Taljedi quarry (Seville, Spain) has been used in this work. The material was sieved to yield a particle size in the range of 160-200 μm. This particle size range is considered as appropriate for the use of circulating fluidized beds as could be the case in the practical application [21, 49, 50].

2.2. Multicycle calcination/carbonation tests

Multicycle calcination/carbonation tests have been carried out by means of thermogravimetry analysis (TGA). A novel homemade thermobalance has been specially assembled to work in a wide range from low pressures up to 5 bar in order to test the material behavior at specific CaL-TCES conditions. Figure 1 shows a schematic diagram and a photograph of the device. The system consists basically of a high sensitivity CI Electronics microbalance ($2x10^{-7}$ g) and a reactor. The reactor is composed of a Watlow heater and a non-porous mullite tube, connected with the microbalance by KF-flanges sealed by means of a clamp and an o-ring. The temperature of the reactor is controlled by placing a thermocouple on the wall of the Watlow heater, and the temperature of the sample is measured using a second thermocouple positioned underneath the sample crucible. A flat ceramic crucible (0.154 cm^3) was used to hold the sample. A vacuum pump and a pressure gauge were incorporated to the system in order to perform the experiments under a controlled CO_2 pressure (absolute pressures of 0.01, 0.1 or 1 bar in the tests carried out in the present work). CO_2 pressure was controlled by means of low-pressure needle valves connected between the vacuum pump and the thermobalance. Rotameters were used to adjust the gas flow through the thermobalance during the experiments.

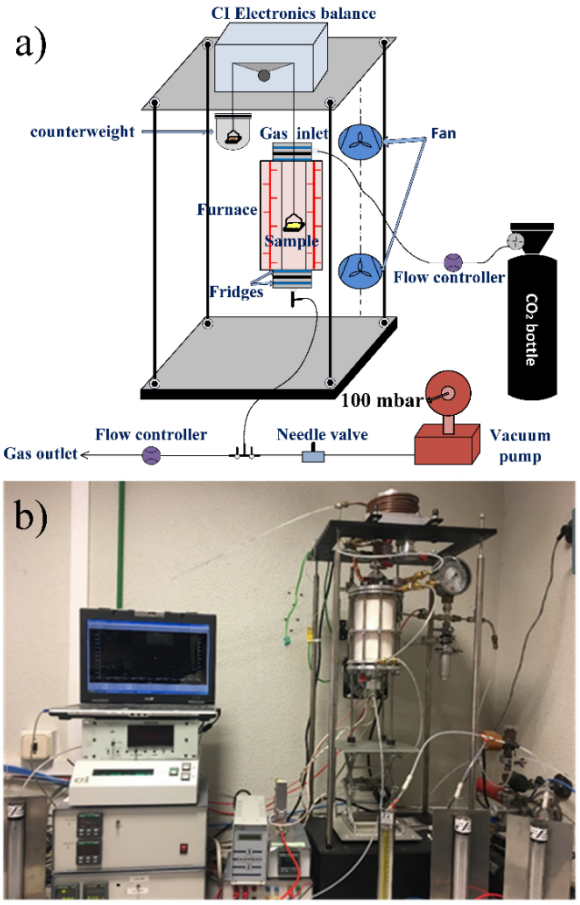

Figure 1. (a) Schematic diagram and (b) photograph of the homemade thermobalance employed in this work.

Mass was accurately calibrated by means of a set of calibration weights ranging from 1 mg to 20 mg. Temperature calibration was performed using the well-known decomposition reaction of hydrous calcium oxalate, which was heated at a heating rate of 10 ºC min^{-1}. Alumina powder was used as a standard to correct buoyancy effects.

Calcination/carbonation tests were carried out in a closed CO_2 cycle. Table 1 lists the diverse operating conditions tested. In this study, carbonation was always performed at an absolute pressure of 1 bar of pure CO_2. According to the thermodynamic equilibrium of the $CaCO_3$/CaO system, the maximum carbonation temperature at these conditions is 895ºC [39, 51, 52]. Three different carbonation temperatures, i.e. 850°C, 765°C and

700°C, were explored with the objective of hastening the carbonation kinetics. Ideally, the higher the carbonation temperature the higher the global efficiency of the CaL-TCES process [14, 16]. However, the reaction kinetics slows down significantly as the equilibrium temperature is approached which is detrimental to the process [14]. Calcination was carried out under an absolute pressure of 1 bar of pure CO_2, as well as under controlled absolute CO_2 pressures of 0.1 bar and 0.01 bar. Calcination temperatures were selected by considering the equilibrium temperatures at these CO_2 pressures (760°C at 0.1 bar and 652°C at 0.01 bar) [39].

Table 1. Operating conditions for the different calcination/carbonation tests carried out in this work, and their corresponding acronyms for their identification throughout the text.

	Calcination		**Carbonation**	
Test	**Temperature (°C)**	**Absolute pressure (bar)**	**Temperature (°C)**	**Absolute pressure (bar)**
T1	**765**	**0.1**	**765**	**1**
T2	**765**		**850**	
T3	**765**	**0.01**	**765**	
T4	**700**		**700**	
T5	**700**		**850**	

Multicycle calcination/carbonation tests were started with a precalcination stage of the limestone sample at the selected CO_2 pressure. As a first step, pressure was reduced by means of the vacuum pump. Once the system was stabilized, the temperature was increased at 10ºC min^{-1} to the selected calcination temperature. After the sample was fully calcined, the temperature was varied at 10ºC min^{-1} rate to the carbonation temperature, and then the CO_2 pressure was increased to an absolute pressure of 1 bar to carry out the carbonation stage (Figure 2). Then, the temperature and the CO_2 pressure were again

changed to the calcination conditions to start a new cycle (Figure 2). Residence times of 10 min as typical of circulating fluidized based processes were employed in both the calcination and carbonation stages.

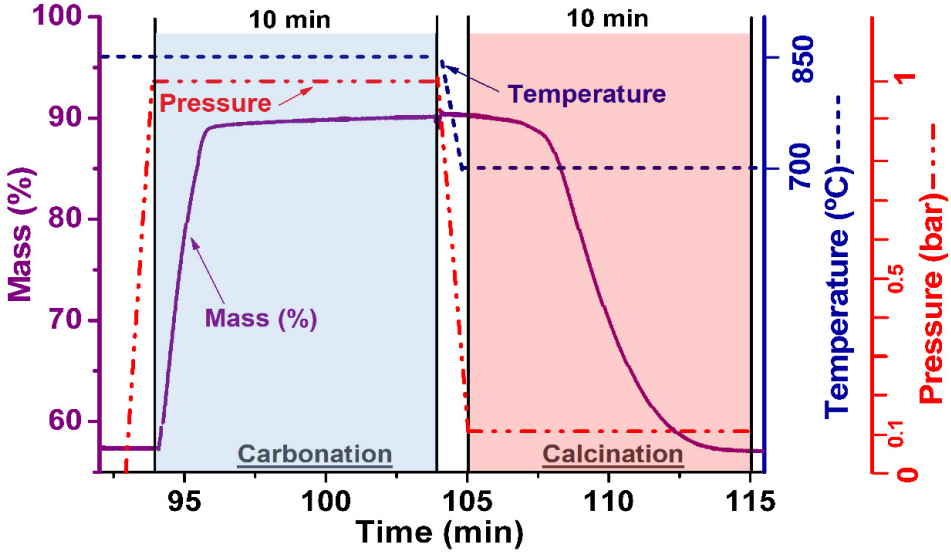

Figure 2. Time evolution of sample mass (%), temperature (°C) and absolute pressure (bar) for a calcination/carbonation cycle of limestone. In this test, carbonation was carried out at 1 bar CO_2 and 850ºC, and calcination at 0.1 bar CO_2 and 700ºC.

The multicycle activity of limestone obtained from tests carried out at the conditions shown in Table 1 was assessed by means of the effective conversion (X_{eff}), defined as the ratio of the mass of CaO converted to $CaCO_3$ in the carbonation stage to the total sample mass before carbonation (Equation 1):

$$X_{eff}(N) = \frac{m_{carbN} - m_N}{m_N} \cdot \frac{W_{CaO}}{W_{CO2}} \qquad (1)$$

Here, m_{CarbN} and m_N are the sample masses after and before carbonation in the N^{th} cycle, and W_{CO2} = 44 g/mol and W_{CaO} = 56 g/mol are the molar masses of CO_2 and CaO, respectively.

As an example, Figure 3 shows a complete thermogram corresponding to the test T2, in which carbonation and calcination were performed at 765ºC and 0.1 bar CO_2, and 850ºC

and 1 bar CO_2, respectively. Remarkably, this figure illustrates that a stable accurate measurement of the sample mass can be achieved with the homemade thermobalance employed in this work, which is of great relevance for the reliability of TGA tests.

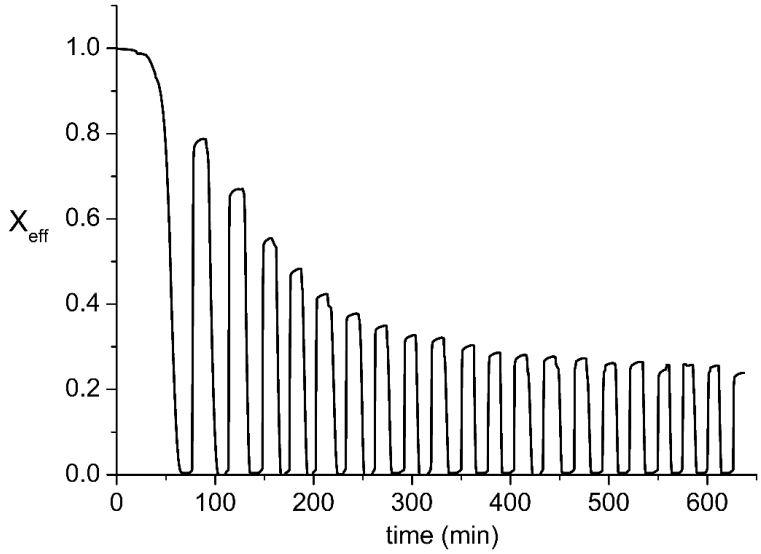

Figure 3. Time evolution of effective conversion (X_{eff}) measured during calcination/carbonation cycles in test T2.

2.3. Sample characterization

Scanning electron microscopy (SEM) was used to analyze the microstructure of the limestone samples after the tests. To this end, a high-resolution Hitachi S4800 SEM-FEG microscope was employed. The samples were gold sputter-coated in an Emitech K5509 Telstar. Total surface areas (BET) and total pore volumes (V_p) of the samples after the first, third and fifth calcinations were measured using an ASAP2420 Micromeritics instrument at -196ºC. Prior to the analysis, the samples were degassed in vacuum at 400ºC for 2 h. The BET equation was used to calculate the total surface areas, while the total pore volume was determined from the amount of N_2 absorbed at a p/p_0 value of 0.97.

Temperature dependent X-ray diffraction patterns were collected in vacuum (0.1 bar) and under a 100 cm^3 min^{-1} airflow using a Philips X'Pert Pro diffractometer equipped with a

high temperature Anton Par camera. The instrument works at 45 kV and 40 mA, using Cu Kα radiation, and is equipped with an X'Celerator detector and a graphite diffracted beam monochromator.

3. Results and discussion

Figure 4 shows data on the multicycle conversion measured under all the calcination/carbonation conditions listed in Table 1. Values of the multicycle conversion of limestone tested under CSP-CO_2 conditions (calcination and carbonation at an absolute pressure of 1 bar CO_2) are included for comparison. In all cases, conversion is enhanced when calcination is carried out at 0.01 bar CO_2 (Figure 4b, tests T3, T4 and T5) as compared to the experiments in which calcination was performed at 0.1 bar CO_2 (Figure 4a, tests T1 and T2). The effect of absolute CO_2 pressure can be inferred from a comparison of experiments T1 and T3, in which both calcination and carbonation were carried out at 765ºC, being the CO_2 pressure the only difference. Higher conversions are consistently attained for the experiment performed at 0.01 bar CO_2. Moreover, full conversion is achieved during the first carbonation. Thus, it is clear that a reduction in the absolute CO_2 calcination environment significantly promotes the multicycle performance of limestone.

The worst multicycle performance is observed for limestone when tested under CSP-CO_2 conditions. Arguably, the high temperatures employed for calcination in these tests (950ºC) greatly enhances CaO sintering, leading to a marked loss of CaO reactivity to carbonation as reported in a previous study [53].

Multicycle CaO effective conversion data fits well to the semiempirical equation (Equation 2) [54-56] as may be seen in Fig. 4:

$$X_N = X_r + \frac{X_1}{\mathrm{k(N-1)+(1-X_r/X_1)^{-1}}};\ (N = 1, 2 \ldots) \qquad (2)$$

where X_r is the residual conversion towards which CaO conversion converges asymptotically after a very large number of cycles, X_1 is CaO conversion at the first cycle, k is the deactivation rate constant and N is the cycle number. Table 2 lists the values obtained for X_r and k for the five tests performed.

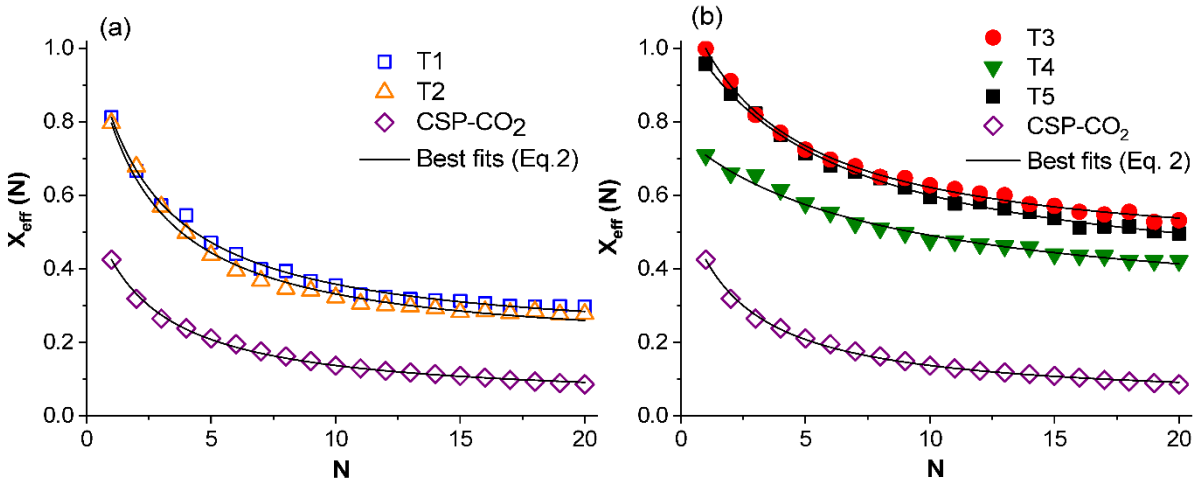

Figure 4. Multicycle effective conversion data measured for natural limestone tested under the calcination/carbonation conditions listed in Table 1. (a) Calcinations under 0.1 bar CO_2. (b) Calcinations under 0.01 bar CO_2. Solid lines represent the best fits of Eq. 2 to data (best fitting parameters are shown in table 2).

Table 2. Values of deactivation rate (k) and residual conversion (X) obtained by fitting Eq. 2 to multicycle conversion experimental data (Fig. 4).

Test	k	Xr
T1	0.40	0.19
T2	0.41	0.17
T3	0.37	0.42
T4	0.18	0.27
T5	0.23	0.34
CSP-CO_2 [53]	0.34	0.04

As may be seen in Figure 4a, only small differences were obtained in the effective conversion after 20 cycles for the samples calcined at 0.1 bar CO_2, independently of the different carbonation temperatures tested. This is also clearly shown in the values of k and X_r derived for these tests (Table 2). Slightly higher conversion values were obtained for the test T1 (calcination and carbonation at 765ºC), with a value of the residual conversion of 0.19. The higher carbonation temperature used in test T2 (850ºC) did not significantly changed conversion data and residual values. This result suggests that higher carbonation temperatures are not detrimental to the CaL performance of limestone under these experimental conditions, which is of interest for the practical application since the overall cycle efficiency is promoted as the carbonation temperature is increased [10, 41]. On the other hand, the experiments in which calcinations were carried out at 0.01 bar CO_2 led to significant differences in the multicycle behavior as depending on the carbonation and calcination temperatures. Thus, in test T4, where both carbonation and calcination were carried out at relatively low temperature (700ºC), the multicycle CaO activity remained low from the first cycle as compared to tests T3 and T5. A value of X_r of 0.27 was estimated for this test. On the other hand, an increase of the carbonation temperature (tests T3 and T5), improved the multicycle activity. Thus, full carbonation was reached in the first cycle cycle ($X_{eff}(1) = 1$) in test T3, while almost full carbonation ($X_{eff}(1) = 0.95$) was attained in test T5. Similar multicycle activity values were obtained for T3 and T5 during the first 9 cycles, although the decay of conversion was fastened after the nineth cycle in the T3 test. The residual value of conversion X_r was 0.42 in test T3 and 0.34 in test T5 (Table 2). Interestingly, as in the experiments carried out at 0.1 bar CO_2, a higher carbonation temperature (850ºC for test T5) did not have an adverse effect on the multicycle activity of limestone. Conversely, decreasing the carbonation temperature (T4 test) resulted in a reduced overall conversion. These observations can be related to results

reported in previous works, where introducing an intermediate recarbonation stage before calcination at high temperature and high CO_2 concentration was proved beneficial to conversion in subsequent carbonation stages provided that the calcination stage was carried out in mild conditions [57, 58].

Time evolution of CaO conversion measured for each test during the carbonation and calcination stages at the 1st and 19th cycles are shown in Figure 5. As well-known carbonation consists of two clearly differentiated stages [54, 59]. The first one is a fast reaction controlled phase that occurs at the surface of the CaO particles [10, 26], which is evidenced in the thermogram by a sharp increase of the mass in a short time period. Carbonation proceeds then by a slower diffusion controlled stage, which is limited by the diffusion of CO_2 through the product layer of $CaCO_3$ built up on the surface of the CaO particles [26, 60]. This is observed in the thermogram as a remarkably slower increase in the sample mass as a function of time [26].

As shown in Figure 5 most of carbonation occurs in the fast reaction-controlled phase when limestone is calcined under absolute low CO_2 pressure despite complete conversion is not achieved in this phase. Arguably, a limiting mechanism that plays also a role is pore-plugging [11]. Pore plugging consists of the rapid formation of a superficial layer of $CaCO_3$ on the external surface of the CaO particle that covers the pores thus hindering the percolation of CO_2 molecules into the internal pores, which hampers conversion in the fast-reaction controlled phase. This undesirable effect is obviously enhanced when working with large particles (> 50 μm) and also when limestone is calcined under mild conditions which leads to the formation of smaller pores more susceptible of being plugged [38, 61]. Since carbonation takes place mostly in the fast phase, the reaction essentially ends in just ~1 min (Figure 5). Therefore, an information of practical value that may be derived from the present work is that very short residence times could be used

for carbonation which would serve to improve the process efficiency [10, 41]. In contrast, it may be seen that calcination occurs at a much slower rate, lasting up to 7 min when carried out at 700ºC (Figure 5d).

Importantly, CaO conversion in the fast reaction-controlled phase is affected by the CO_2 pressure used for calcination. As may be seen in Figure 5a CaO conversion does not depend on the carbonation temperature when calcination is carried out under 0.1 bar. Thus, very similar values of X_{eff} were obtained in the first cycle for the tests carried out at different carbonation temperatures, namely, 765ºC (T1) and 850ºC (T2). On the other hand, a significant drop of conversion with the number of cycles in the fast reaction-controlled phase is seen (Figure 4a), which suggest that the CaO grains suffer severe sintering during calcinations at 0.1 bar CO_2. Nevertheless, this drop of conversion is less pronounced than that of the sample tested under CSP-CO_2 conditions (Figure 4a). Since carbonation temperatures are similar under both types of conditions, CaO multicycle deactivation could be attributed to the enhancement of sintering by calcination at the very high temperature needed when it is carried out under 1 bar CO_2 (CSP-CO_2 conditions).

As seen in Figures 4b and 5c CaO conversion is very high when calcination takes place at 0.01 bar CO_2. Moreover, as aforementioned, it is clear from Figure 5c that in these tests conversion is affected by the temperature of carbonation already from the first cycle. Thus, the samples carbonated at 765ºC and 850ºC show the highest conversion, while the sample carbonated at 700ºC yields a conversion as low as 0.68 in the first cycle. These differences fade away with the number of cycles (Figures 4b and 5d).

According to these results, it can be argued that the use of low CO_2 pressures in the calciner environment enhances significantly the CaO multicycle activity by efficiently mitigating CaO sintering. Accordingly, carbonation in the fast phase, which is directly related to the CaO surface area available, is kept at a relatively high value even after 19

cycles (Figures 5b and 5d). Compared with typical conversion values so far reported in previous TGA studies on CaL for TCES [15, 38, 53], our results show considerably higher values of conversion.

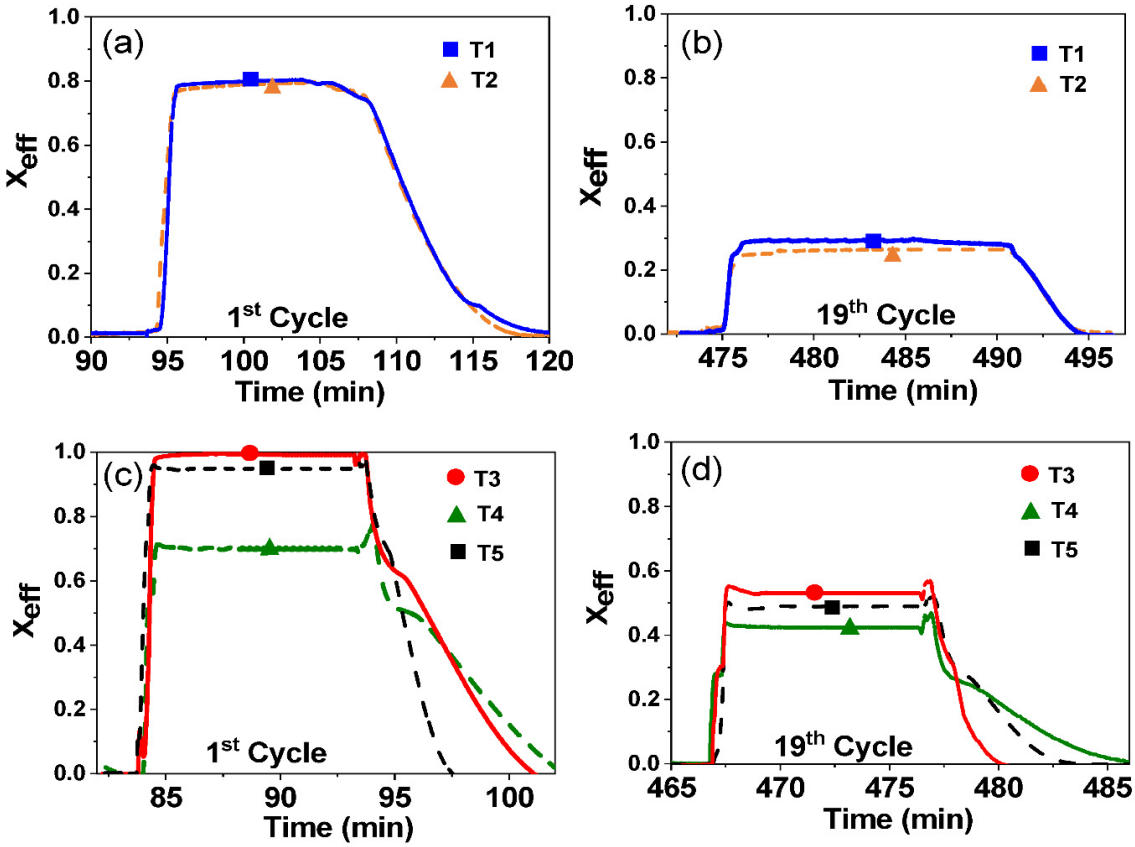

Figure 5. Time evolution of CaO conversion during the carbonation and calcination stages of the 1st and 19th cycles for the different tests. (a, b) Calcinations under 0.1 bar CO_2. c) and d) Calcinations under 0.01 bar CO_2.

To get further insight on the enhanced multicycle performance of limestone when calcination is carried out under absolute low CO_2 pressures, the samples were characterized using several techniques.

SEM and TEM micrographs (Figures 6 and 7) show the microstructure of the samples after the first calcination (Figure 6) and after 20 cycles ending by calcination (Figure 7),

carried out under T1 (Figures 6a and 6b) and T3 (Figures 6c and 6d) conditions. Since carbonation and calcination temperatures are identical, any microstructural differences could only be attributed to the different CO_2 pressures used for calcination. The microstructure displayed by CaO samples after the first calcination looks very similar despite the different absolute CO_2 pressures (0.1 bar and 0.01 bar). The surface of the particles is composed of nanometric CaO grains as may be observed in Figures 6b and 6d. It is also readily apparent that calcination under low CO_2 pressure leads to microstructures with very small pores (Figures 6a and 6c).

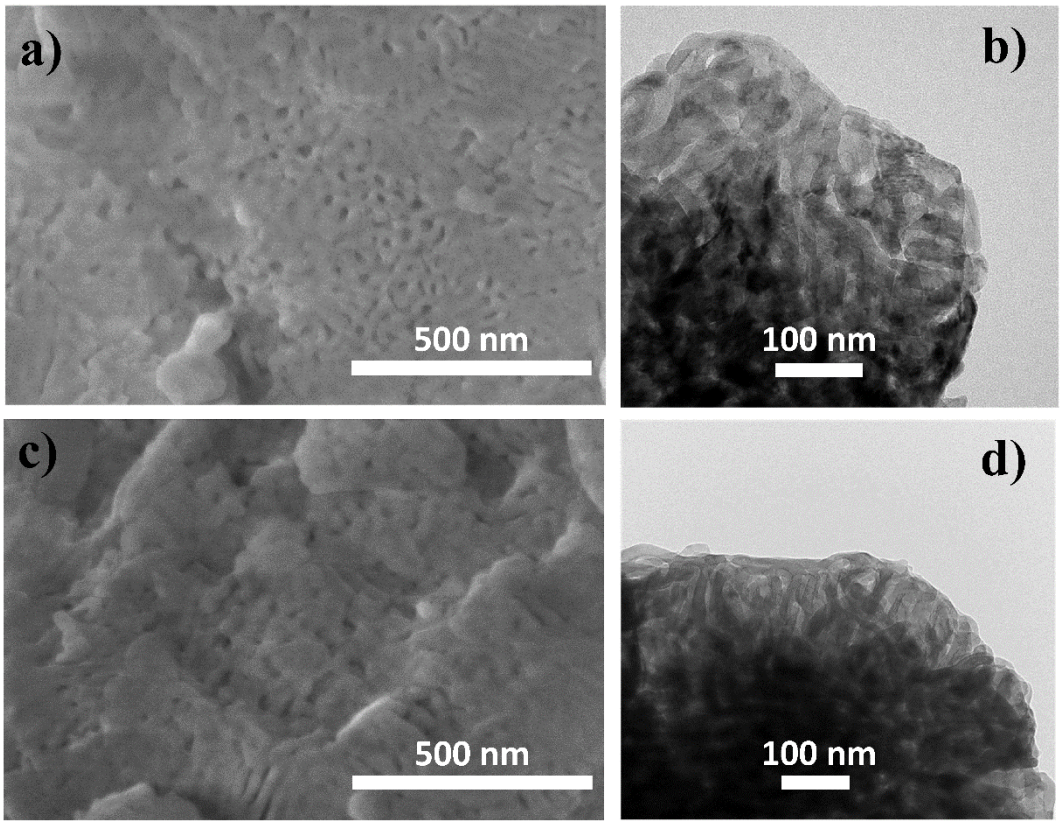

Figure 6. SEM and TEM micrographs of CaO derived from natural limestone after one calcination stage at 765 ºC and under an absolute CO_2 pressure of (a, b) 0.1 bar (test T1), and (c, d) 0.01 bar (test T3).

The microstructure of the samples drastically changes after 20 cycles (Figure 7). Thus, the size of the CaO grains show marked sintering after the cycles at 765 ºC, which would lead to a significant decrease in the surface area available for carbonation in the fast reaction-controlled phase as revealed by the TGA tests. This effect is much more noticeable when calcinations were performed under a CO_2 pressure of 0.1 bar (Figures 7a and 7b).

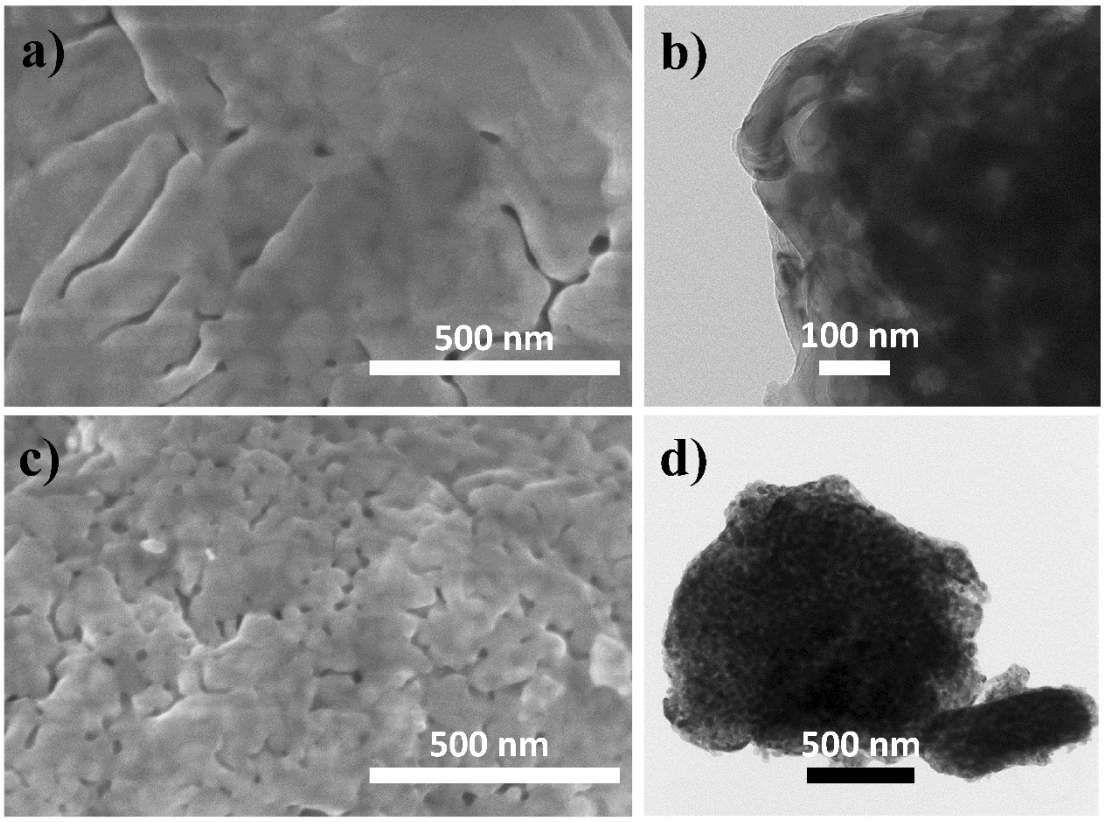

Figure 7. SEM and TEM micrographs of CaO derived from natural limestone after 20 cycles at 765 ºC. (a, b) 0.1 bar (test T1), and (c, d) 0.01 bar (test T3).

SEM and TEM observations were complemented by surface area (BET) and pore volume measurements (V_p). These parameters were determined for the CaO samples after the first calcination and after the third and fifth cycles ending in calcination, carried out under the

conditions corresponding to tests T1 and T3. Results of these measurements are collected in Table 3 together with the corresponding conversion values measured by TGA (Figure 4). For example, after the first calcination, conversion values obtained in the first carbonation for tests T1 and T3 are 0.81 and 1.00, respectively. Surface area and pore volume after calcination are higher for the sample tested under the operating conditions of test T3, as compared to the sample tested under the operating conditions of T1. Thus, it is clear that calcining under an absolute pressure of 0.01 bar CO_2 leads to an increased surface area available for carbonation as would be expected from the TGA results. Then, the favorable carbonation conditions used (high temperature and high CO_2 concentration) promotes carbonation in the fast reaction-controlled phase.

The characterization analysis indicates that the high conversion values obtained from the first carbonation cycle for test T3 (Figures 4 and 5) are a consequence of the effect of the calcination conditions on the CaO microstructure (Figures 6 and 7). CaO surface area and therefore conversion are higher for operating conditions corresponding to test T1.

Table 3. Specific surface area (S_{BET}) and porosity data (V_p) of the CaO samples, measured after the first, third and fifth cycles under the conditions corresponding to tests T1 and T3.

	Calcination/carbonation Test					
	T1 (T = 765ºC; carbonation at 1 bar CO_2, calcination at 0.1 bar CO_2)			**T3 (T = 765ºC; carbonation at 1 bar CO_2, calcination at 0.01 bar CO_2)**		
Calcination	**S_{BET} ($m^2\ g^{-1}$)**	**V_p ($cm^3\ g^{-1}$)**	**X_{eff}**	**S_{BET} ($m^2\ g^{-1}$)**	**V_p ($cm^3\ g^{-1}$)**	**X_{eff}**
1	55.5	0.161	0.81	74.9	0.225	1.00
3	16.2	0.075	0.57	17.7	0.091	0.82
5	9.6	0.047	0.47	14.6	0.077	0.72

In order to investigate the effect of the absolute gas pressure in the calciner environment on the microstructure of the nascent CaO, temperature dependent XRD tests were carried in which limestone samples were calcined under vacuum (0.01 bar) and in air (absolute pressure of 1 bar and a flux of 100 cm^3/min). The CaO crystallite size of the samples calcined in vacuum and in airflow at 765ºC were estimated using the Scherrer method. This temperature was used as a reference because, as discussed above, the multicycle experiments performed at 765ºC provide the best results in terms of CaO conversion (tests T1 and T3).

Figure 8 shows a comparison of the main diffraction peak (2 0 0) corresponding to CaO ($2\theta = 37.3^{o}$) calcined in vacuum and in air, respectively. It is clear from the figure that the peak width is greater for the sample calcined under vacuum. Moreover, the intensity of the diffraction peak is higher for the sample calcined in air. The Shcherrer equation gives a CaO crystallite size of 13 nm for the sample calcined in vacuum and 24 nm for the sample calcined in air. Thus, the absolute pressure in the calciner environment has an important effect on the size of the CaO crystallites and therefore on CaO reactivity.

Similar results were reported by Beruto and Searcy [62], who furthermore correlated the size of CaO crystals resulting from limestone calcination to the reactivity of the calcined limestone towards hydroxylation. More recently, the reactivity of CaO towards carbonation that results from the crystallographic $CaCO_3$/CaO transformation has been observed to be inversely correlated to the size of CaO crystallites [63, 64].

In situ XRD analysis reported elsewhere [64] indicates that the growth of CaO crystallites occurs through two stages. The first stage is driven by the aggregation of nascent CaO nanocrystals that attract each other by surface van der Waals forces, which is followed by sintering of the aggregated nanocrystals. Arguably, calcination under high CO_2 partial pressure enhances the adsorption of CO_2 molecules on the surface of the nascent CaO

nanocrystals which increases the strength of van der Waals attractive forces between them thus enhancing aggregation. Accordingly, by reducing the CO_2 absolute pressure in the calciner environment, CO_2 adsorption is minimized which diminishes the strength of surface attractive forces thus hindering aggregation of CaO nanocrystals. Thus, a favorable strategy to boost the reactivity of the CaO regenerated in each cycle after calcination under CO_2 would be to reduce the absolute CO_2 pressure to avoid aggregation of the nascent CaO nanocrystals and shorten the calcination time to minimize subsequent sintering. As confirmed by the TGA results reported in the present work reducing the CO_2 pressure is a highly efficient technique to mitigate the loss of CaO reactivity after calcination.

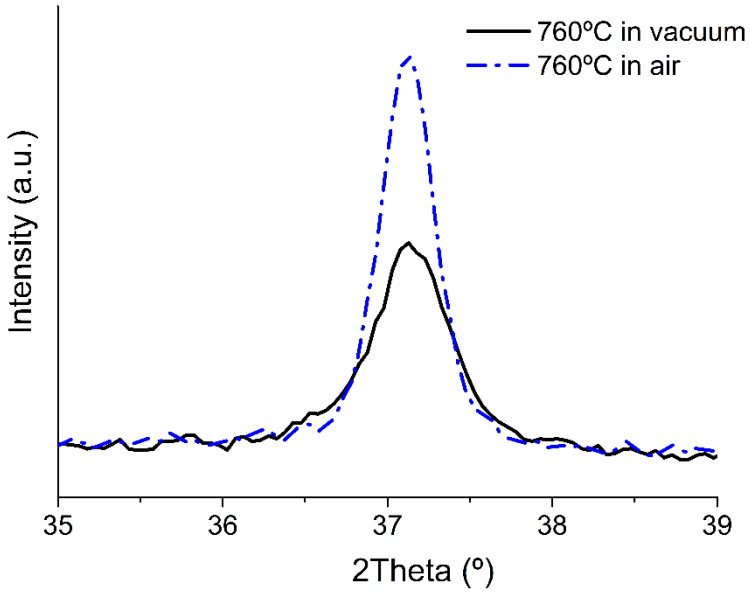

Figure 8. Comparison of the main diffraction peak (2 0 0) corresponding to CaO (2θ = 37.3º) for limestone samples calcined in vacuum and in air at 765ºC.

4. Conclusions

In this work, the multicyclic performance of natural limestone has been investigated when subjected to novel Calcium Looping conditions for thermochemical energy storage in CSP plants with tower technology. These conditions involve a CO_2 closed circuit for carbonation and calcination, which would reduce the technical complexity of the technology. The main novelty lies in calcining at absolute low pressures of CO_2 (0.01 and 0.1 bar) whereas carbonation is performed at high temperature under CO_2 at atmospheric pressure as proposed in previous schemes.

A main benefit of carrying out the calcination stage at reduced CO_2 pressure is that the temperature to achieve full calcination in short residence times can be substantially decreased, which would facilitate the design of the solar reactor. Furthermore, our study demonstrates that the absolute CO_2 pressure used for calcination has an important effect on the multicyclic CaO conversion. Thus, calcining at low CO_2 pressures enhances notably conversion and mitigates its progressive decay with the number of cycles.

The highest values of effective conversion were obtained for limestone samples calcined at an absolute pressure of 0.01 bar of CO_2 at 765ºC whereas carbonation is carried out at 850ºC under CO_2 at atmospheric pressure as corresponding to CaL conditions for thermochemical energy storage in CSP plants. The residual conversion that results from these conditions is enhanced by a factor of 10 compared to that obtained when calcination is carried out under CO_2 at atmospheric pressure. SEM, TEM, specific surface area (S_{BET}) and temperature dependent XRD measurements indicate that the enhancement of CaO conversion is correlated to the microstructure of calcined CaO samples. Calcination under reduced CO_2 pressure leads to a decreased size of the CaO grains thus increasing the surface area available for carbonation in the fast reaction-controlled phase. Enhanced

carbonation takes place in very short residence times, which would allow shortening the residence time of the CaO solids in the carbonator.

5. Acknowledgements

This work has been supported by the Spanish Government Agency Ministerio de Economía y Competitividad (contracts CTQ2017-83602-C2-1-R and -2-R) and Junta de Andalucía-Consejería de Economía, Conocimiento, Empresas y Universidad-Fondo Europeo de Desarrollo Regional (FEDER) (Programa Operativo FEDER Andalucía 2014-2020, project US-1262507). We also acknowledge the funding received by the European Union's Horizon 2020 research and innovation programme under grant agreement No. 727348, project SOCRATCES.

6. References

1 C. Prieto, P. Cooper, A. I. Fernandez, L. F. Cabeza, Review of technology: Thermochemical energy storage for concentrated solar power plants, Renew. Sust. Energ. Rev. 60 (2016) 909-929.

2 L. Andre, S. Abanades, G. Flamant, Screening of thermochemical systems based on solid-gas reversible reactions for high temperature solar thermal energy storage, Renew. Sust. Energ. Rev. 64 (2016) 703-715.

3 J. Cot-Gores, A. Castell, L. F. Cabeza, Thermochemical energy storage and conversion: A-state-of-the-art review of the experimental research under practical conditions, Renew. Sust. Energ. Rev. 16 (2012) 5207-5224.

4 X. Y. Chen, Z. Zhang, C. G. Qi, X. Ling, H. Peng, State of the art on the high-temperature thermochemical energy storage systems, Energy Conv. Manag. 177 (2018) 792-815.

5 P. Pardo, A. Deydier, Z. Anxionnaz-Minvielle, S. Rouge, M. Cabassud, P. Cognet, A review on high temperature thermochemical heat energy storage, Renew. Sust. Energ. Rev. 32 (2014) 591-610.

6 N. S. Lewis, Research opportunities to advance solar energy utilization, Science 351 (2016) aad1920.

7 S. E. B. Edwards, V. Materic, Calcium looping in solar power generation plants, Sol. Energy 86 (2012) 2494-2503.

8 R. Chacartegui, A. Alovisio, C. Ortiz, J. M. Valverde, V. Verda, J. A. Becerra, Thermochemical energy storage of concentrated solar power by integration of the calcium looping process and a CO_2 power cycle, Appl. Energy 173 (2016) 589-605.

9 C. Ortiz, R. Chacartegui, J. M. Valverde, A. Alovisio, J. A. Becerra, Power cycles integration in concentrated solar power plants with energy storage based on calcium looping, Energy Conv. Manag. 149 (2017) 815-829.

10 A. Alovisio, R. Chacartegui, C. Ortiz, J. M. Valverde, V. Verda, Optimizing the CSP-Calcium Looping integration for Thermochemical Energy Storage, Energy Conv. Manag. 136 (2017) 85-98.

11 M. Benitez-Guerrero, B. Sarrion, A. Perejon, P. E. Sanchez-Jimenez, L. A. Perez-Maqueda, J. Manuel Valverde, Large-scale high-temperature solar energy storage using natural minerals, Sol. Energy Mater. Sol. Cells 168 (2017) 14-21.

12 J. M. Valverde, J. Miranda-Pizarro, A. Perejón, P. E. Sánchez-Jiménez, L. A. Pérez-Maqueda, Calcium-Looping performance of steel and blast furnace slags

for thermochemical energy storage in concentrated solar power plants, J. CO2 Util. 22 (2017) 143-154.

13 M. Benitez-Guerrero, J. M. Valverde, A. Perejon, P. E. Sanchez-Jimenez, L. A. Perez-Maqueda, Low-cost Ca-based composites synthesized by biotemplate method for thermochemical energy storage of concentrated solar power, Appl. Energy 210 (2018) 108-116.

14 C. Ortiz, J. M. Valverde, R. Chacartegui, L. A. Perez-Maqueda, Carbonation of Limestone Derived CaO for Thermochemical Energy Storage: From Kinetics to Process Integration in Concentrating Solar Plants, ACS Sustain. Chem. Eng. 6 (2018) 6404-6417.

15 B. Sarrión, A. Perejón, P. E. Sánchez-Jiménez, L. A. Pérez-Maqueda, J. M. Valverde, Role of calcium looping conditions on the performance of natural and synthetic Ca-based materials for energy storage, J. CO2 Util. 28 (2018) 374-384.

16 C. Ortiz, J. M. Valverde, R. Chacartegui, L. A. Perez-Maqueda, P. Giménez, The Calcium-Looping ($CaCO_3$/CaO) process for thermochemical energy storage in Concentrating Solar Power plants, Renew. Sust. Energ. Rev. 113 (2019) 109252.

17 Y. Da, Y. Xuan, L. Teng, K. Zhang, X. Liu, Y. Ding, Calcium-based composites for direct solar-thermal conversion and thermochemical energy storage, Chem. Eng. J. 382 (2020) 122815.

18 S. Yasipourtehrani, S. Tian, V. Strezov, T. Kan, T. Evans, Development of robust CaO-based sorbents from blast furnace slag for calcium looping CO_2 capture, Chem. Eng. J. 387 (2020) 124140.

19 J. Blamey, E. J. Anthony, J. Wang, P. S. Fennell, The calcium looping cycle for large-scale CO_2 capture, Prog. Energy Combust. Sci. 36 (2010) 260-279.

20 C. C. Dean, J. Blamey, N. H. Florin, M. J. Al-Jeboori, P. S. Fennell, The calcium looping cycle for CO_2 capture from power generation, cement manufacture and hydrogen production, Chem. Eng. Res. Des. 89 (2011) 836-855.

21 D. P. Hanak, E. J. Anthony, V. Manovic, A review of developments in pilot-plant testing and modelling of calcium looping process for CO_2 capture from power generation systems, Energy Environ. Sci. 8 (2015) 2199-2249.

22 A. Perejon, L. M. Romeo, Y. Lara, P. Lisbona, A. Martinez, J. M. Valverde, The Calcium-Looping technology for CO_2 capture: On the important roles of energy integration and sorbent behavior, Appl. Energy 162 (2016) 787-807.

23 P. Lisbona, A. Martinez, L. M. Romeo, Hydrodynamical model and experimental results of a calcium looping cycle for CO_2 capture, Appl. Energy 101 (2013) 317-322.

24 I. Martinez, G. Grasa, J. Parkkinen, T. Tynjala, T. Hyppanen, R. Murillo, M. C. Romano, Review and research needs of Ca-Looping systems modelling for post-combustion CO_2 capture applications, Int. J. Greenh. Gas Control 50 (2016) 271-304.

25 B. Arias, M. E. Diego, J. C. Abanades, M. Lorenzo, L. Diaz, D. Martinez, J. Alvarez, A. Sanchez-Biezma, Demonstration of steady state CO_2 capture in a 1.7 MWth calcium looping pilot, Int. J. Greenh. Gas Control 18 (2013) 237-245.

26 C. Ortiz, R. Chacartegui, J. M. Valverde, J. A. Becerra, L. A. Perez-Maqueda, A new model of the carbonator reactor in the calcium looping technology for post-combustion CO_2 capture, Fuel 160 (2015) 328-338.

27 M. E. Diego, B. Arias, M. Alonso, J. C. Abanades, The impact of calcium sulfate and inert solids accumulation in post-combustion calcium looping systems, Fuel 109 (2013) 184-190.

28 J. M. Valverde, Ca-based synthetic materials with enhanced CO_2 capture efficiency, J. Mater. Chem. A 1 (2013) 447-468.

29 M. E. Diego, B. Arias, A. Mendez, M. Lorenzo, L. Diaz, A. Sanchez-Biezma, J. C. Abanades, Experimental testing of a sorbent reactivation process in La Pereda 1.7 MWth calcium looping pilot plant, Int. J. Greenh. Gas Control 50 (2016) 14-22.

30 J. M. Valverde, P. E. Sanchez-Jimenez, L. A. Perez-Maqueda, Calcium-looping for post-combustion CO_2 capture. On the adverse effect of sorbent regeneration under CO_2, Appl. Energy 126 (2014) 161-171.

31 H. L. Zhang, J. Baeyens, J. Degreve, G. Caceres, Concentrated solar power plants: Review and design methodology, Renew. Sust. Energ. Rev. 22 (2013) 466-481.

32 A. G. Fernandez, S. Ushak, H. Galleguillos, F. J. Perez, Development of new molten salts with $LiNO_3$ and $Ca(NO_3)_2$ for energy storage in CSP plants, Appl. Energy 119 (2014) 131-140.

33 A. Bonk, S. Sau, N. Uranga, M. Hernaiz, T. Bauer, Advanced heat transfer fluids for direct molten salt line-focusing CSP plants, Prog. Energy Combust. Sci. 67 (2018) 69-87.

34 V. Encinas-Sanchez, M. T. de Miguel, M. I. Lasanta, G. Garcia-Martin, F. J. Perez, Electrochemical impedance spectroscopy (EIS): An efficient technique for monitoring corrosion processes in molten salt environments in CSP applications, Sol. Energy Mater. Sol. Cells 191 (2019) 157-163.

35 A. G. Fernandez, B. Munoz-Sanchez, J. Nieto-Maestre, A. Garcia-Romero, High temperature corrosion behavior on molten nitrate salt-based nanofluids for CSP plants, Renew. Energy 130 (2019) 902-909.

36 E. González-Roubaud, D. Pérez-Osorio, C. Prieto, Review of commercial thermal energy storage in concentrated solar power plants: Steam vs. molten salts, Renew. Sust. Energ. Rev. 80 (2017) 133-148.

37 B. Sarrion, J. M. Valverde, A. Perejon, L. Perez-Maqueda, P. E. Sanchez-Jimenez, On the Multicycle Activity of Natural Limestone/Dolomite for Thermochemical Energy Storage of Concentrated Solar Power, Energy Technol. 4 (2016) 1013-1019.

38 M. Benitez-Guerrero, J. M. Valverde, P. E. Sanchez-Jimenez, A. Perejon, L. A. Perez-Maqueda, Multicycle activity of natural $CaCO_3$ minerals for thermochemical energy storage in Concentrated Solar Power plants, Sol. Energy 153 (2017) 188-199.

39 I. Barin, *Thermochemical Data of Pure Substances*, Federal Republic of Germany, 1989.

40 C. Tregambi, F. Montagnaro, P. Salatino, R. Solimene, A model of integrated calcium looping for CO_2 capture and concentrated solar power, Sol. Energy 120 (2015) 208-220.

41 C. Ortiz, M. C. Romano, J. M. Valverde, M. Binotti, R. Chacartegui, Process integration of Calcium-Looping thermochemical energy storage system in concentrating solar power plants, Energy 155 (2018) 535-551.

42 C. Tregambi, P. Salatino, R. Solimene, F. Montagnaro, An experimental characterization of Calcium Looping integrated with concentrated solar power, Chem. Eng. J. 331 (2018) 794-802.

43 M. Liu, N. H. Steven Tay, S. Bell, M. Belusko, R. Jacob, G. Will, W. Saman, F. Bruno, Review on concentrating solar power plants and new developments in high

temperature thermal energy storage technologies, Renew. Sust. Energ. Rev. 53 (2016) 1411-1432.

44 Y. A. Criado, A. Huille, S. Rougé, J. C. Abanades, Experimental investigation and model validation of a $CaO/Ca(OH)_2$ fluidized bed reactor for thermochemical energy storage applications, Chem. Eng. J. 313 (2017) 1194-1205.

45 C. Tregambi, C. Bevilacqua, M. Troiano, R. Solimene, P. Salatino, A novel autothermal fluidized bed reactor for concentrated solar thermal applications, Chem. Eng. J. 398 (2020) 125702.

46 J. M. Valverde, S. Medina, Reduction of Calcination Temperature in the Calcium Looping Process for CO_2 Capture by Using Helium: In Situ XRD Analysis, ACS Sustain. Chem. Eng. 4 (2016) 7090-7097.

47 C. Ortiz, J. Manuel Valverde, R. Chacartegui, L. A. Pérez-Maqueda, P. Gimenez-Gavarrell, Scaling-up the Calcium-Looping Process for CO_2 Capture and Energy Storage, KONA Powder Part. J. advpub (2021).

48 D. T. Beruto, A. W. Searcy, M. G. Kim, Microstructure, kinetic, structure, thermodynamic analysis for calcite decomposition: free-surface and powder bed experiments, Thermochim. Acta 424 (2004) 99-109.

49 J. C. Abanades, D. Alvarez, Conversion limits in the reaction of CO_2 with lime, Energy Fuels 17 (2003) 308-315.

50 M. J. Espin, F. J. Duran-Olivencia, J. M. Valverde, Role of particle size on the cohesive behavior of limestone powders at high temperature, Chem. Eng. J. 391 (2020) 123520.

51 E. H. Baker, The calcium oxide–carbon dioxide system in the pressure range 1-300 atmospheres, J. Chem. Soc. (Resumed) (1962) 464-470.

52 F. Garcia-Labiano, A. Abad, L. F. de Diego, P. Gayan, J. Adanez, Calcination of calcium-based sorbents at pressure in a broad range of CO_2 concentrations, Chem. Eng. Sci. 57 (2002) 2381-2393 Pii s0009-2509(02)00137-9.

53 B. Sarrion, P. E. Sanchez-Jimenez, A. Perejon, L. A. Perez-Maqueda, J. M. Valverde, Pressure Effect on the Multicycle Activity of Natural Carbonates and a Ca/Zr Composite for Energy Storage of Concentrated Solar Power, ACS Sustain. Chem. Eng. 6 (2018) 7849-7858.

54 J. M. Valverde, A model on the CaO multicyclic conversion in the Ca-looping process, Chem. Eng. J. 228 (2013) 1195-1206.

55 J. M. Valverde, P. E. Sanchez-Jimenez, A. Perejon, L. A. Perez-Maqueda, CO_2 multicyclic capture of pretreated/doped CaO in the Ca-looping process. Theory and experiments, Phys. Chem. Chem. Phys. 15 (2013) 11775-11793.

56 G. S. Grasa, J. C. Abanades, CO_2 Capture Capacity of CaO in Long Series of Carbonation/Calcination Cycles, Ind. Eng. Chem. Res. 45 (2006) 8846-8851.

57 J. M. Valverde, P. E. Sanchez-Jimenez, L. A. Perez-Maqueda, Effect of Heat Pretreatment/Recarbonation in the Ca-Looping Process at Realistic Calcination Conditions, Energy Fuels 28 (2014) 4062-4067.

58 J. M. Valverde, P. E. Sanchez-Jimenez, L. A. Perez-Maqueda, M. A. S. Quintanilla, J. Perez-Vaquero, Role of crystal structure on CO_2 capture by limestone derived CaO subjected to carbonation/recarbonation/calcination cycles at Ca-looping conditions, Appl. Energy 125 (2014) 264-275.

59 D. Alvarez, J. C. Abanades, Determination of the Critical Product Layer Thickness in the Reaction of CaO with CO_2, Ind. Eng. Chem. Res. 44 (2005) 5608-5615.

60 Z. Sun, S. Luo, P. Qi, L.-S. Fan, Ionic diffusion through Calcite ($CaCO_3$) layer during the reaction of CaO and CO_2, Chem. Eng. Sci. 81 (2012) 164-168.

61 J. D. Duran-Martin, P. E. S. Jimenez, J. M. Valverde, A. Perejon, J. Arcenegui-Troya, P. G. Trinanes, L. A. P. Maqueda, Role of particle size on the multicycle calcium looping activity of limestone for thermochemical energy storage, J. Adv. Res. 22 (2020) 67-76.

62 D. Beruto, A. W. Searcy, Calcium oxides of high reactivity, Nature 263 (1976) 221-222.

63 M. Benitez-Guerrero, J. M. Valverde, A. Perejon, P. E. Sanchez-Jimenez, L. A. Perez-Maqueda, Effect of milling mechanism on the CO_2 capture performance of limestone in the Calcium Looping process, Chem. Eng. J. 346 (2018) 549-556.

64 J. M. Valverde, S. Medina, Crystallographic transformation of limestone during calcination under CO_2, Phys. Chem. Chem. Phys. 17 (2015) 21912-21926.